

SUPPORTING INFORMATION

Structure and composition define immunorecognition of nucleic acid nanoparticles

Enping Hong¹, Justin R. Halman², Ankit B. Shah¹, Emil F. Khisamutdinov³, Marina A. Dobrovolskaia^{1*}, Kirill A. Afonin^{2,4*}

¹ Nanotechnology Characterization Lab, Cancer Research Technology Program, Leidos Biomedical Research Inc., Frederick National Laboratory for Cancer Research, Frederick, MD 21702, USA

² Nanoscale Science Program, Department of Chemistry, the University of North Carolina at Charlotte, Charlotte, NC 28223, USA

³ Department of Chemistry, Ball State University, Muncie, IN 47306, USA

⁴ The Center for Biomedical Engineering and Science, the University of North Carolina at Charlotte, Charlotte, NC 28223, USA

* To whom correspondence should be addressed: Marina A. Dobrovolskaia, phone: 301-228-4935, email: marina@mail.nih.gov; Kirill A. Afonin, phone: 1-704-687-0685, fax: 1-704-687-0960, email: kafonin@uncc.edu.

NANP compositions used in this project:

Molecular weights (g/mol) of all NANPs were calculated and are shown in parentheses.

RNA and DNA polygons [1]:

RNA Triangle 5'→3' (76208.3)

rT1: GGAUGCUGGUACUUUUGAAACAUUUCGAGUCGCGAGGGUUUCCCAUCGUUGGCCCGUAUCGCGUUUUCUUAUGAAGA
rT2: GGUCGCGACCUUCUUUCCUCGCGACUCGAAAUGUUUCUUUCGAGGUCGCC
rT3: GGAUCUUUCGCUUUUCGCGAUACGGGCCAACGAUGGGUUUUGAAGGUCGCGAC
rT4: GGGCGACCUUCUUUUGUACCAGCAUCCUCUUCUAUAAGUUUUGGCGAAAGAUC

RNA Square 5'→3' (101133.1)

rS1: GGAUGCUGGUACUUUUGUUGGCCGAGACCAUAUCCCGUUUUGAAACAUUUCGAGUCGCGAGGGUUUCCCAUCGUUGGCCCGUAUCGCGUUU
UCUUAUGAAGA
rT2: GGUCGCGACCUUCUUUCCUCGCGACUCGAAAUGUUUCUUUCGAGGUCGCC
rT3: GGAUCUUUCGCUUUUCGCGAUACGGGCCAACGAUGGGUUUUGAAGGUCGCGAC
rT4: GGGCGACCUUCUUUUGUACCAGCAUCCUCUUCUAUAAGUUUUGGCGAAAGAUC
rS5: GGGCGACCUUCUUUCCGGGAUAUGGUCUCGGCCAACUUUCGAGGUCGCC

RNA Pentagon 5'→3' (126057.8)

rP1: GGAUGCUGGUACUUUUGUUGGCCGAGACCAUAUCCCGUUUUGGGCCAACUCUUAGCGUGUCGCUUUUGAAACAUUUCGAGUCGCGAGGGUUU
UCCCAUCGUUGGCCCGUAUCGCGUUUUCUUAUGAAGA
rT2: GGUCGCGACCUUCUUUCCUCGCGACUCGAAAUGUUUCUUUCGAGGUCGCC
rT3: GGAUCUUUCGCUUUUCGCGAUACGGGCCAACGAUGGGUUUUGAAGGUCGCGAC
rT4: GGGCGACCUUCUUUUGUACCAGCAUCCUCUUCUAUAAGUUUUGGCGAAAGAUC
rS5: GGGCGACCUUCUUUCCGGGAUAUGGUCUCGGCCAACUUUCGAGGUCGCC
rP6: GGGCGACCUUCUUUCCGGACACGCUAAGAGUUGGCCUUUUCGAGGUCGCC

RNA Hexagon 5'→3' (150981.6)

rH1: GGAUGCUGGUACUUUUGUUGGCCGAGACCAUAUCCCGUUUUGGGCCAACUCUUAGCGUGUCGCUUUUGGGGCCGAUAUCGAACCGGGUUGUUU
UGAAACAUUUCGAGUCGCGAGGGUUUCCCAUCGUUGGCCCGUAUCGCGUUUUCUUAUGAAGA
rT2: GGUCGCGACCUUCUUUCCUCGCGACUCGAAAUGUUUCUUUCGAGGUCGCC
rT3: GGAUCUUUCGCUUUUCGCGAUACGGGCCAACGAUGGGUUUUGAAGGUCGCGAC
rT4: GGGCGACCUUCUUUUGUACCAGCAUCCUCUUCUAUAAGUUUUGGCGAAAGAUC
rS5: GGGCGACCUUCUUUCCGGGAUAUGGUCUCGGCCAACUUUCGAGGUCGCC
rP6: GGGCGACCUUCUUUCCGGACACGCUAAGAGUUGGCCUUUUCGAGGUCGCC
rH7: GGGCGACCUUCUUUACCCGGUUCGAUAUCGGCCUUUUCGAGGUCGCC

DNA Triangle 5'→3' (73450.5)

dT1: GGATGCTGGTACTTTTGAACATTTTCGAGTCGCGAGGGTTTTCCCATCGTTGGCCCGTATCGCGTTTTCTTATGAAGA
dT2: GGTGCGACCTTCTTTTCCCTCGGACTCGAAATGTTTCTTTTCGAGGTCGCC
dT3: GGATCTTTCGCCTTTTTCGCGATACGGGCCAACGATGGGTTTTGAAGGTCGCGAC
dT4: GGGCGACCTCGTTTTGTACCAGCATCCTTTCATAAGTTTTGGCGAAAGATCC

DNA Square 5'→3' (97435.9)

dS1: GGATGCTGGTACTTTTGTGGCCGAGACCATATCCCGTTTTTGAACATTTTCGAGTCGCGAGGGTTTTCCCATCGTTGGCCCGTATCGCGTTTT
TCTTATGAAGA
dT2: GGTGCGACCTTCTTTTCCCTCGGACTCGAAATGTTTCTTTTCGAGGTCGCC
dT3: GGATCTTTCGCCTTTTTCGCGATACGGGCCAACGATGGGTTTTGAAGGTCGCGAC
dT4: GGGCGACCTCGTTTTGTACCAGCATCCTTTCATAAGTTTTGGCGAAAGATCC
dS5: GGGCGACCTCGTTTTCCGGGATATGGTCTCGGCCAACTTTTCGAGGTCGCC

DNA Pentagon 5'→3' (121421.3)

dP1: GGATGCTGGTACTTTTGTGGCCGAGACCATATCCCGTTTTTGGGCCAACTCTTAGCGTGTCCGTTTTGAAACATTTTCGAGTCGCGAGGGTTTT
TCCCATCGTTGGCCCGTATCGCGTTTTCTTATGAAGA
dT2: GGTGCGACCTTCTTTTCCCTCGGACTCGAAATGTTTCTTTTCGAGGTCGCC
dT3: GGATCTTTCGCCTTTTTCGCGATACGGGCCAACGATGGGTTTTGAAGGTCGCGAC
dT4: GGGCGACCTCGTTTTGTACCAGCATCCTTTCATAAGTTTTGGCGAAAGATCC
dS5: GGGCGACCTCGTTTTCCGGGATATGGTCTCGGCCAACTTTTCGAGGTCGCC
dP6: GGGCGACCTCGTTTTCCGGACACGCTAAGAGTTGGCCTTTTTCGAGGTCGCC

DNA Hexagon 5'→3' (145407.8)

dH1: GGATGCTGGTACTTTTGTGGCCGAGACCATATCCCGTTTTTGGGCCAACTCTTAGCGTGTCCGTTTTGGGGCCGATATCGAACCGGTGTTTT
TGAACATTTTCGAGTCGCGAGGGTTTTCCCATCGTTGGCCCGTATCGCGTTTTCTTATGAAGA
dT2: GGTGCGACCTTCTTTTCCCTCGGACTCGAAATGTTTCTTTTCGAGGTCGCC
dT3: GGATCTTTCGCCTTTTTCGCGATACGGGCCAACGATGGGTTTTGAAGGTCGCGAC
dT4: GGGCGACCTCGTTTTGTACCAGCATCCTTTCATAAGTTTTGGCGAAAGATCC
dS5: GGGCGACCTCGTTTTCCGGGATATGGTCTCGGCCAACTTTTCGAGGTCGCC

dP6: GGGCGACCTCGTTTTTCGGACACGCTAAGAGTTGGCCCTTTTCGAGGTCGCC
dH7: GGGCGACCTCGTTTTTCACCCGGTTCGATATCGGCCCTTTTCGAGGTCGCC

RNA and DNA cubes and anti-cubes with 3 ssNTs per strand per each corner [2]:

RNA cube with three Us at each corner 5'→3' (98968.5)

rA: GGCAACUUUGAUCCUCGGUUUAGCGCCGGCCUUUCUCCACACUUUCACG
rB: GGGAAUUUCGUGGUAGGUUUUGUUGCCCGUGUUUCUACGAUUACUUUGGUC
rC: GGACAUUUUCGAGACAGCAUUUUUCCCGACUUUGCGGAUUGUAUUUAGG
rD: GGGCUUUUGACCUUCUGCUUUUAGUCCCUUAUUUCUUAUAGACUUUUGGCC
rE: GGGAGAUUUAGUCAUUUAGUUUACAUCGCUUUUGUAUUCGUAUUUGUGU
rF: GGGAUUUUACCUACCGUUUUUGCUGUCUGUUUGCAGAAGGUCUUUCGA
rD-AF488: GGGCUUUUGACCUUCUGCUUUUAGUCCCUUAUUUCUUAUAGACUUUUGGCC-AF488

RNA anticube with three As at each corner 5'→3' (105428.2)

anti-rA: GGGGUGAAAGUGUGGGAGAAAAGCCGGCGCUAAAACCGAGGGAUCAAGUUGCC
anti-rB: GGGACCAAAGUAAUCGUAGAAACACGGGCAACAAAACCUACCACGAAUUUCC
anti-rC: GGACUAAAAUACAUCGCAAGGUCGGGAAAAAUGCUGUCUGGAAAAUGUCC
anti-rD: GGCCAAAAGUCAUUUAGAAAUAGGGGACAUAAAAGCAGAAGGUCAAAAGCGCC
anti-rE: GGACACAAACUACGAUUACAAGCGGAUUUUAUAAAACUUAUAGACUAAAUCUCC
anti-rF: GGGAUCCGAAAGACCUUCUGCAAACGAGACAGCAAACGUGGUAGGUAAGAUC

DNA cube with three Ts at each corner 5'→3' (95688)

dA: GGCAACTTTGATCCCTCGGTTTAGCGCCGGCCTTTTCTCCACACTTTTCACG
dB: GGGAAATTTGCTGGTAGGTTTTGTGCGCGTGTCTTACGATTACTTTGGTC
dC: GGACATTTTCGAGACAGCATTTTTTCCCGACCTTTGCGGATTGATTTTAGG
dD: GGGCCTTTTGACCTTCTGCTTTATGTCCCTATTCTTAATGACTTTTGGCC
dE: GGGAGATTTAGTCATTAAGTTTACAATCCGCTTTGTAATCGTAGTTTGTGT
dF: GGGATCTTTACCTACCAGTTTTGCTGTCTCGTTGCGAAGGCTTTCCGA
dD-AF488: GGGCCTTTTGACCTTCTGCTTTATGTCCCTATTCTTAATGACTTTTGGCC-AF488

DNA anticube with three As at each corner 5'→3' (96336.9)

anti-dA: CGTGAAAGTGTGGGAGAAAAGCCGGCGCTAAACCGAGGGATCAAAGTTGCC
anti-dB: GACCAAAGTAATCGTAGAAACACGGGCAACAAAACCTACCACGAAATTTCC
anti-dC: CCTAAAATACAATCCGCAAAGGTCCGGAAAAAATGCTGTCTCGAAAATGTCC
anti-dD: GGCCAAAAGTCATTAAGAAATAGGGACATAAAGCAGAAGGTCAAAGCGCC
anti-dE: ACACAAACTACGATTACAAGCGGATTGTAAAACCTAATGACTAAATCTCC
anti-dF: TCGGAAAGACCTTCTGCAAACGAGACAGCAAACCTGGTAGGTAAGATCC
anti-dC-AF488: AF488-CCTAAAATACAATCCGCAAAGGTCCGGAAAAAATGCTGTCTCGAAAATGTCC

RNA cubes with 1 and 2 ssNTs per strand per each corner [3]:

RNA cube with two Us at each corner 5'→3'

rA: GGCAACUUUGAUCCUCGGUUAGCGCCGGCCUUUCUCCACACUUUCACG
rB: GGGAAUUUCGUGGUAGGUUUUGUUGCCCGUGUUUCUACGAUUACUUUGGUC
rC: GGACAUUUUCGAGACAGCAUUUUUCCCGACCUUGCGGAUUGUAUUUAGG
rD: GGGCUUUUGACCUUCUGCUUUUAGUCCCUUAUUUCUUAUAGACUUUUGGCC
rE: GGGAGAUUUAGUCAUUUAGUUUACAUCGCUUUUGUAUUCGUAUUUGUGU
rF: GGGAUUUUACCUACCGUUUUGCUGUCUGUUUGCAGAAGGUCUUUCGA

RNA cube with one Us at each corner 5'→3'

rA: GGCAACUGAUCCUCGGUAGCGCCGGCCUUUCUCCACACUCACG
rB: GGGAAUUCGUGGUAGGUUUUGUUGCCCGUGUCUACGAUUACUUGGUC
rC: GGACAUUCGAGACAGCAUUUUUCCCGACCUUGCGGAUUGUAUUUAGG
rD: GGGCUUUGACCUUCUGCUUUUAGUCCCUUAUUUCUUAUAGACUUUUGGCC
rE: GGGAGAUAGUCAUUUAGUUUACAUCGCUUUUGUAUUCGUAUUUGUGU
rF: GGGAUUCUACCUACCGUUUUGCUGUCUGUUUGCAGAAGGUCUUUCGA

RNA ring, RNA anti-ring, and RNA ring/anti-ring fibers [2]:

RNA ring 5'→3' (84759)

nrA: GGGAACCGUCCACUGGUUCCCGCUACGAGAGCCUGCCUCGUAGC
nrB: GGGAACCGCAGGCUUGUCCCGCUACGAGAGACGCCUCGUAGC
nrC: GGGAACCGCGUUCUGGUUCCCGCUACGAGACGUCUCCUCGUAGC
nrD: GGGAACCGAGACGUGGUUCCCGCUACGAGUCGUGGUCUCGUAGC
nrE: GGGAACCAACCACGAGGUUCCCGCUACGAGAACCAUCCUCGUAGC
nrF: GGGAACCGAUGGUUGGUUCCCGCUACGAGAGUGGACCUUCGUAGC
nrC-AF488: GGGAACCGCGUUCUGGUUCCCGCUACGAGACGUCUCCUCGUAGC-AF488

RNA anti-ring 5'→3' (94923.2)

anti-nrA: GGGAAAGCUACGAGGCAGGCUCUCGUAGCGGGAAACCAGUGGACGGUUCUUCC
anti-nrB: GGGAAAGCUACGAGGCAGGCUCUCGUAGCGGGAAACCAGCCUGCGGUUUCUUCC
anti-nrC: GGGAAAGCUACGAGGAGACGUCUCGUAGCGGGAAACCAGAACGCGGUUUCUUCC
anti-nrD: GGGAAAGCUACGAGACCACGACUCGUAGCGGGAAACCAGUCUCGGUUCUUCC
anti-nrE: GGGAAAGCUACGAGGAUGGUUCUCGUAGCGGGAAACCUCGUGGUGGUUUCUUCC
anti-nrF: GGGAAAGCUACGAGGUCCACUCUCGUAGCGGGAAACCAACCAUCGGUUCUUCC
anti-nrA-AF488: GCUACGAGGCAGGCUCUCGUAGCGGGAAACCAGUGGACGGUUCUUCC-AF488

RNA ring/anti-ring monomers assembly 5'→3'

nrA: GGGAAACGUCCACUGGUUCCCGCUACGAGAGCCUGCCUCGUAGC
anti-nrA: GGGAAAGCUACGAGGCAGGCUCUCGUAGCGGGAAACCAGUGGACGGUUCUUCC

RNA nanoring with 6 ssNTs gaps 5'→3' (73382.3)

6nts_nrA: GGGAGUCCACUUCUCCGGCUAGACGAGAGCCUGCCUCGU
6nts_nrB: GGGAGCAGGCUUCUCCGGCUAGACGAGAGAACGCCUCGU
6nts_nrC: GGGAGCGUUCUUCUCCGGCUAGACGAGACGUCUCUCCUCGU
6nts_nrD: GGGAGAGACGUUCUCCGGCUAGACGAGUCGUGGUCUCGU
6nts_nrE: GGGAAACCAGAUCCCGGCUAGACGAGAGAACCAUCCUCGU
6nts_nrF: GGGAGAUGGUUUCUCCGGCUAGACGAGAGUGGACCCUCGU

RNA/DNA fibers:

Asymmetric 25/27mer Dicer substrate [4] 5'→3'

Sense: pACCCUGAAGUUAUCUGCACCACCG
Antisense: CGGUGGUGCAGAUGAACUUCAGGGUCA

DNA strands for hybrid fibers 5'→3'

Fiber with sense 1: AAGGGATTCCCTCGGTGGTGCAGATGAACTTCAGGGTCATCCCTAAAGGGA
Fiber with sense 2: AGGGAAATCCCTTCGGTGGTGCAGATGAACTTCAGGGTCATCCCTTTAGGGAA
Fiber with antisense 1: TCCCTTTAGGGAAATGACCCCTGAAGTTCATCTGCACCACCGAGGGAAATCCCTT
Fiber with antisense 2: TTCCTAAAGGGATGACCCTGAAGTTCATCTGCACCACCGAAGGGATTCCCTT

RNA/DNA polygons:

Asymmetric 25/27mer Dicer substrate [4] 5'→3'

Sense: pACCCUGAAGUUAUCUGCACCACCG
Antisense: CGGUGGUGCAGAUGAACUUCAGGGUCA

DNA strands for hybrid polygons 5'→3'

Polygon with sense: AAGGGATTCCCTCGGTGGTGCAGATGAACTTCAGGGTCAAGGGAAATCCCTT
Polygon with antisense: AAGGGATTCCCTTGACCCTGAAGTTCATCTGCACCACCGAGGGAAATCCCTT

RNA fibers (with HIV-1-like kissing loops) 5'→3':

A: GGGAAUCCAAGGAGGCAGGAUUCUCCGUCACAGAAGGAGGCACUGUGAC
B: GGGAAACGUAAAGCCUCCAACGUUCCCGGAUGCUAAGCCUCCAAGCAUCC
B-AF488: GGGAAACGUAAAGCCUCCAACGUUCCCGGAUGCUAAGCCUCCAAGCAUCC-AF488

RNA 3WJ domain from phi29 pRNA (17243.3) [5] 5'→3':

a3WJ: UUGCCAUGUGUAUGUGGG
b3WJ: CCCACAUACUUUGUUGAUCC
c3WJ: GGAUCAAUCAUGGCAA

DNA tetrahedron (67896.9) [6] 5'→3':

Strand 1: ACATTCCTAAGTCTGAAACATTACAGCTTGCTACACGAGAAGAGCCGCCATAGTA
Strand 2: TATCACCAGGCAGTTGACAGTGTAGCAAGCTGTAATAGATGCCGAGGGTCCAATAC
Strand 3: TCAACTGCCTGGTGATAAAAACGACACTACGTGGGAATCTACTATGGCGGCTCTTC
Strand 4: TTCAGACTTAGGAATGTGCTTCCCACGTAGTGTGTTGTATTGGACCCTCGCAT

SUPPORTING METHODS

RNA synthesis and purification. All DNAs, all fluorescently labeled oligos, and some RNAs were purchased from Integrated DNA Technologies (IDTDNA.com). All non-purchased RNAs were synthesized via *in vitro* run-off transcription with T7 RNA polymerase. Prior to *in vitro* transcription, the DNAs' templates and primers (with embedded T7 promoter sequences) were polymerase chain reaction (PCR)–amplified (MyTaq, Bioron), then column-purified (Zymo Research). *In vitro* transcription was performed by incubating DNA templates at 37°C for 3.5 hours in the presence of T7 RNA polymerase, 300 mM DTT, 400 mM HEPES-KOH, 10 mM spermidine, and 120 mM MgCl₂. The reaction was stopped by incubation with RQ1 DNase (Promega) for 30 minutes at 37°C, and then the templates were purified by an 8 M urea polyacrylamide gel (urea-PAGE, 8% acrylamide) by extracting gel slices and eluting them into 300 mM NaCl, 1X Tris-borate-EDTA overnight. The following day, the eluted RNAs were added to a 2X volume of 100% ethanol and cooled to -20°C for 1–3 hours. RNAs were precipitated in 2.5 volumes of 100% ethanol, rinsed with 90% ethanol, vacuum-dried, and dissolved in endotoxin-free water (HyClone). The concentrations of the samples were determined using a NanoDrop2000.

NANPs' synthesis. All NANPs were synthesized via one-pot assembly of constituent strands at an equimolar concentration (normally, to have NANPs at 1 μM). Several different assembly protocols were used to maximize the yields of the produced NANPs. All NANPs were assembled in an assembly buffer: 89 mM Tris-borate (1xTB), 2 mM MgCl₂, 50 mM KCl. Following all assembly protocols, all samples were confirmed via non-denaturing polyacrylamide gel electrophoresis, native-PAGE (8% acrylamide (37.5:1), 1xTB, 2 mM MgCl₂), and visualized with a Bio-Rad ChemiDoc MP System using total staining with ethidium bromide or fluorescently labeled oligonucleotides. Gels were run in a cold room at 300 V, 150 mA, for 30 minutes.

DNA and RNA cubes and anti-cubes were assembled by mixing all constituent strands in endotoxin-free water at an equimolar concentration and heating to 95°C for two minutes. The samples were then snap-cooled to 45°C and incubated for two minutes. Finally, 5X assembly buffer was added to reach the appropriate concentration, and the samples were incubated at 45°C for an additional 30 minutes.

RNA rings, anti-rings, ring/anti-ring monomers, and RNA fibers were assembled by mixing all strands in endotoxin-free water at an equimolar concentration and heating to 95°C for two minutes. The samples were then snap-cooled on ice for two minutes, after which 5X assembly buffer was added and the samples were incubated for 30 minutes at 30°C.

RNA and DNA triangles, squares, pentagons, hexagons, and the three-way junction motif of ϕ29 pRNA were assembled by mixing all constituent strands in the presence of the assembly buffer. The samples were assembled in a thermal cycler (Bio-Rad) by heating to 80°C for 10 minutes, then cooling to 4°C at a rate of 0.4°C per second.

The DNA tetrahedron was assembled in a thermal cycler (Bio-Rad) by heating to 95°C for five minutes, then cooling to 20°C at a rate of 0.4°C per second. Because the tetrahedrons were designed to assemble in a much higher concentration of salt, they needed to be further purified.

DNA fibers and polygons with embedded RNA strands were assembled by mixing all constituent strands and heating them to 95°C for two minutes. The samples were then snap-cooled for 20 minutes to room temperature, and the assembly buffer was added.

Studies of NANP structural integrity upon binding and release from Lipofectamine 2000 (L2K). To study the preservation of NANPs' structure following the binding and release from L2K, 10 μL of each NANP (at various concentrations) was mixed with 1 μL of L2K for 30 minutes at room temperature. Following the 30-minute binding incubation, samples were treated with 1 μL of Triton X-100, a detergent that disrupts the structure of L2K and releases the NANPs. Samples were then analyzed by ethidium bromide total staining native-PAGE.

Effects of scavenger receptor inhibitors on NANPs. Alexa Fluor 488 (AF488)–labeled RNA cubes and rings were treated with various scavenger receptor inhibitors to study their effect on naked NANPs and on NANPs complexed with L2K. First, the RNA NANPs (10 nM) were incubated with 1 μ L of L2K for 30 minutes at room temperature. All NANPs (10 nM) were then treated with the various inhibitors (50 μ g/mL) and incubated at room temperature for 30 minutes. Samples were analyzed by native-PAGE.

NANPs' visualization by atomic force microscopy. Freshly cleaved mica was modified with 1-(2-aminoropyl) silatrane according to established protocols. Following mica preparation, 5 μ L of NANPs at various concentrations were deposited onto the modified mica for two minutes. Unbound nucleic acids and excess salts were washed twice with 50 μ L of deionized water, and the mica surface was dried with argon gas. Atomic force microscopy imaging was performed on a MultiMode AFM Nanoscope IV system (Bruker Instruments, Santa Barbara, CA) in tapping mode. Images were recorded with a 1.5-Hz scanning rate using a TESPA-300 probe from Bruker, a resonance frequency of 320 Hz, and a spring constant of 40 N/m. Images were processed using FemtoScan Online (Advanced Technologies Center, Moscow, Russia).

Electroporation of PBMCs with NANPs. NANPs were electroporated using the Neon[®] Transfection System (Invitrogen, Carlsbad, CA) according to the manufacturer's instructions. Electroporation settings were optimized by mock electroporation of PBMCs and assessing viability by AOPI staining; parameters that yielded >90% viability were tested further for the electroporation of AF488-labeled DNA duplexes. The lowest voltage capable of yielding the highest cell viability and DNA transfection was 1X 2350 V, 20 ms pulse, which was used for all electroporation studies. Prior to electroporation, PBMCs were resuspended at 10×10^6 cells/mL in electroporation buffer T. Then, 100 μ L of cells was mixed with 10 pmol of nanoparticles and electroporated with a single 2350 V, 20 ms pulse. Electroporated cells were then immediately transferred to RPMI medium and supplemented with 10% FBS and 2 mM L-glutamine, but without antibiotics. If any additional stimulation was required (i.e., ODN 2216), cells were rested for one hour before adding reagents. Electroporated PBMCs were cultured at 1×10^6 /mL overnight before assaying for viability by AOPI and collecting supernatants for cytokine assays.

Phenotyping of purified DC subsets. After purification of DC subsets, between 50,000 to 200,000 cells per donor were stained with antibodies and isotype controls to determine post-isolation purity. The following antibodies were used: BDCA-2 APC, CD1c FITC, BDCA-3 PE, and REA(S) PE isotype control (Miltenyi Biotec GmbH, Bergisch Gladbach, Germany), as well as CD14 FITC, mouse IgG1 APC isotype control, and mouse IgG2a FITC isotype control (eBioscience, San Diego, CA). Antibodies were diluted in 1% FBS in PBS, and cells were stained for 30 minutes at room temperature. Cells were then washed with 1X PBS and fixed in 2% formaldehyde before analysis by flow cytometry.

siRNA validation in Toll-like receptor (TLR) reporter cells. TLR reporter cells were seeded in six-well plates at 100,000 cells per well and allowed to adhere overnight in Dulbecco's Modified Eagle Medium with 10% FBS. The next day, the medium was switched out for Accell delivery medium with 1% FBS and Accell control or TLR-specific siRNAs at 1 μ M. An equivalent volume of nuclease-free water was used as a negative control. Cells were cultured for a further 72 hours at 37°C. After incubation with siRNA, cells were either tested for secreted embryonic alkaline phosphatase (SEAP) response using TLR agonists or collected for Western blot analysis of TLR expression. Specific TLR agonists were used as follows: 1 μ g/mL Poly(I:C) (TLR3), 5 μ g/mL Imiquimod (TLR7), 100 ng/mL TL8-506 (TLR8), and 10 μ g/mL ODN 2006 (TLR9) (all from Invivogen, San Diego, CA).

Cell viability assay. TLR reporter cells were assayed for cell viability after stimulation with TLR agonists. After incubation with agonists for 24 hours, cells were treated with 20 μ L CellTiter Blue reagent per 100 μ L of media. Cells were incubated for 1–2 hours at 37°C. Then, supernatants were collected and assayed for fluorescence in 96-well black clear-bottomed plates at 560 nm excitation / 590 nm emission.

Western blot of TLR reporter cells. siRNA-treated TLR reporter cells were washed with 1X HBSS and pelleted. The cell pellets were incubated with radioimmunoprecipitation assay (RIPA) buffer (Boston BioProducts, Ashland) that was supplemented with Halt™ Protease and Phosphatase Inhibitor Cocktail

(Thermo Fisher Scientific, Waltham, MA) for 10 min at 4°C. The partially lysed cells were sonicated for 10 seconds at one amplitude to completely lyse the cellular organelles and centrifuged at 15,000g for five minutes to remove debris. Lysate protein concentrations were measured by a BCA protein assay kit (Thermo Fisher Scientific, Waltham, MA), and 10 µg protein was loaded on Novex 4–20% Tris-Glycine gels. After gel electrophoresis, samples were transferred on polyvinylidene difluoride membranes overnight. Membranes were blocked in 5% nonfat milk in PBS-T (0.075% Tween 20 in PBS) overnight at 4°C to reduce nonspecific signals. Blots were probed for appropriate targets using primary and secondary antibodies, and protein bands were visualized using BM Chemiluminescence Western Blotting Substrate (POD) (Roche, Basel, Switzerland). The blot images were acquired using G:Box Chemi XX9 gel documentation system and GeneSys software from Syngene USA (Frederick, MD). All the images were adjusted for brightness and contrast throughout the blots before band intensity quantification with ImageJ software. Relative changes in target proteins were calculated by normalizing the intensity of target proteins, with β actin as loading control, then comparing treated samples with vehicle control.

Additional inhibitor studies. All oligonucleotide-based TLR inhibitors were used at 10 µM and 1 µM. The inhibitors used were as follows: ODN 2088, ODN 2087, ODN 20958, and ODN 20959 (Miltenyi Biotec GmbH, Bergisch Gladbach, Germany), as well as ODN TTAGGG, ODN TTAGGG control, G-ODN, and G-ODN control (Invivogen, San Diego, CA). The small-molecule TLR3 inhibitor Merck 614310 (Millipore Sigma, St Louis, MO) was tested at 30 µM, 10 µM, and 1 µM.

SUPPORTING FIGURES

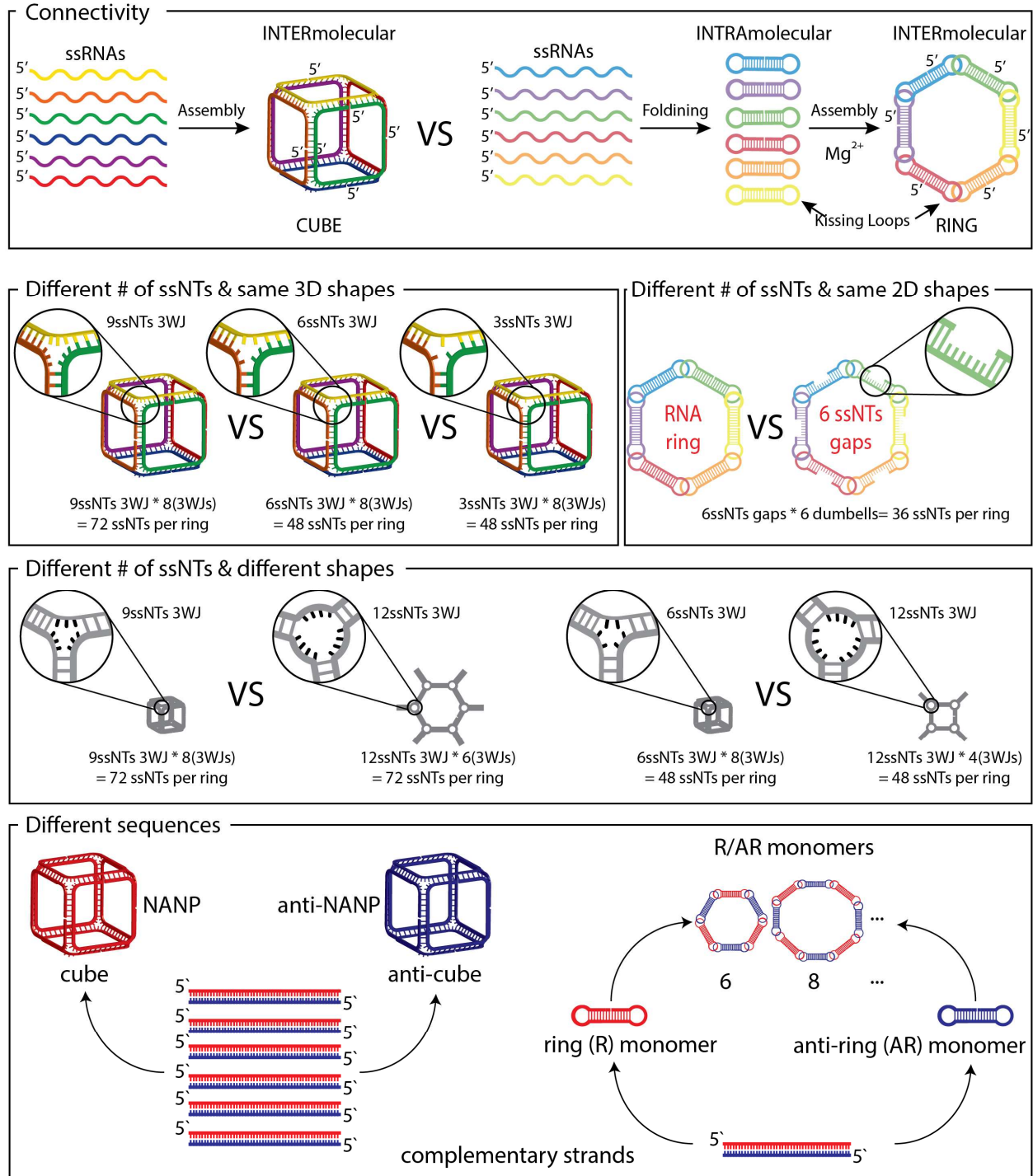


Figure S1: Schematic representation demonstrating NANPs' connectivity and shapes, as well as different sizes of single-stranded nucleotide (ssNTs) linkers on their structures and different sequences resulting in the same 3D shapes.

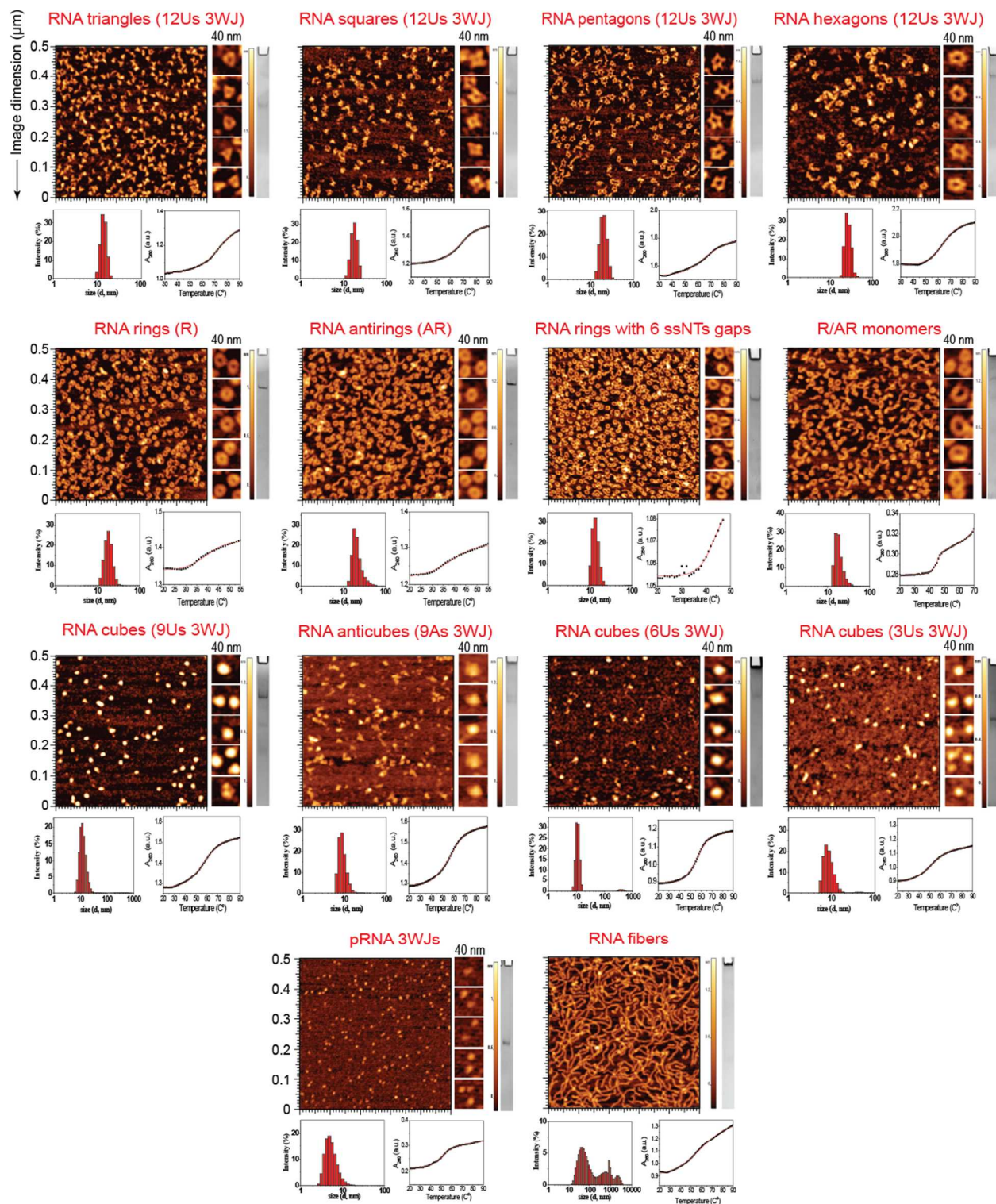


Figure S2. All assemblies of RNA NANPs were confirmed by native-PAGE and visualized by atomic force microscopy. The sizes of NANPs were measured by dynamic light scattering and melting temperatures assessed with ultraviolet-melting experiments.

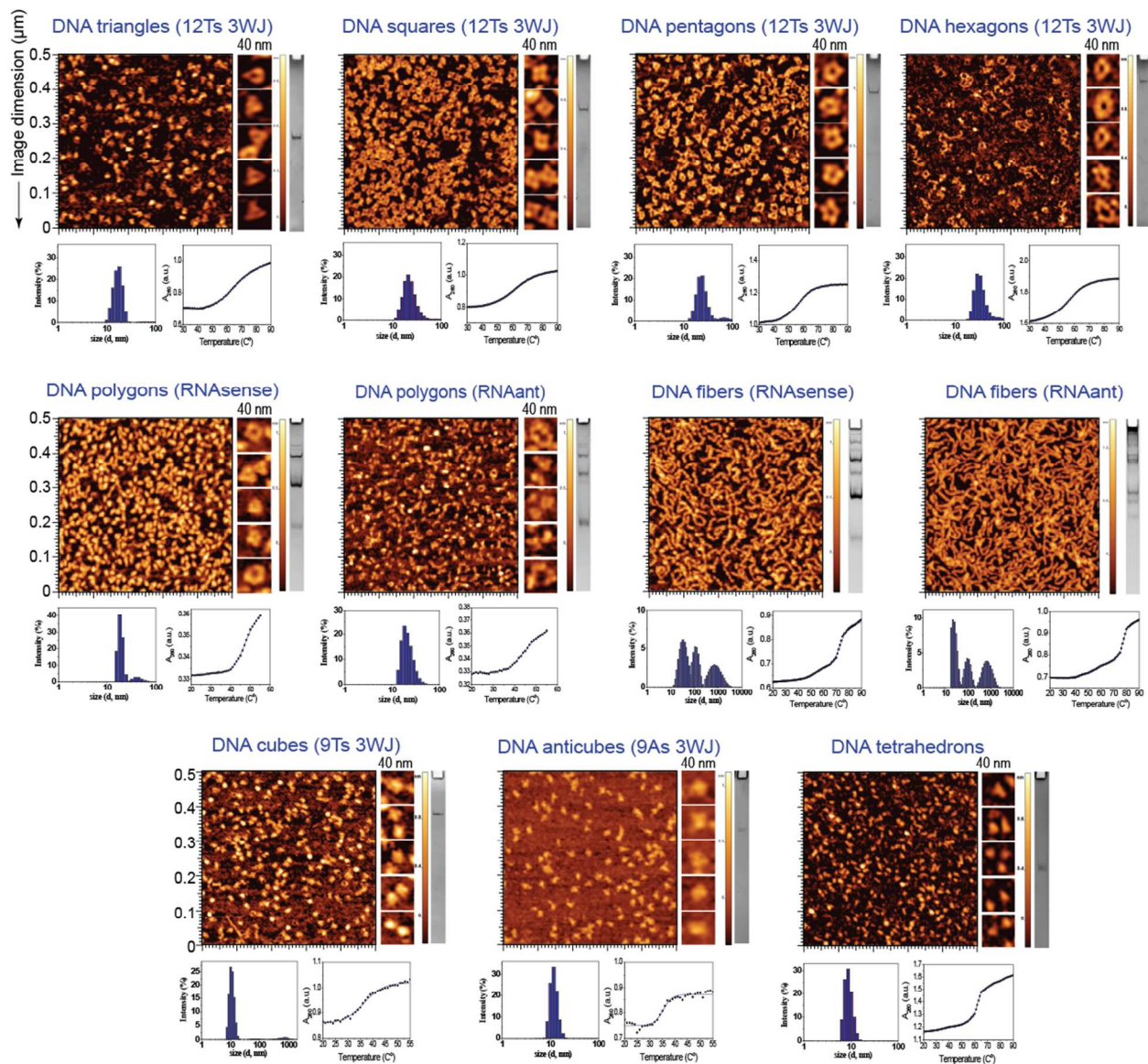


Figure S3. All assemblies of DNA NANPs were confirmed by native-PAGE and visualized by atomic force microscopy. The sizes of NANPs were measured by dynamic light scattering and melting temperatures assessed with ultraviolet-melting experiments.

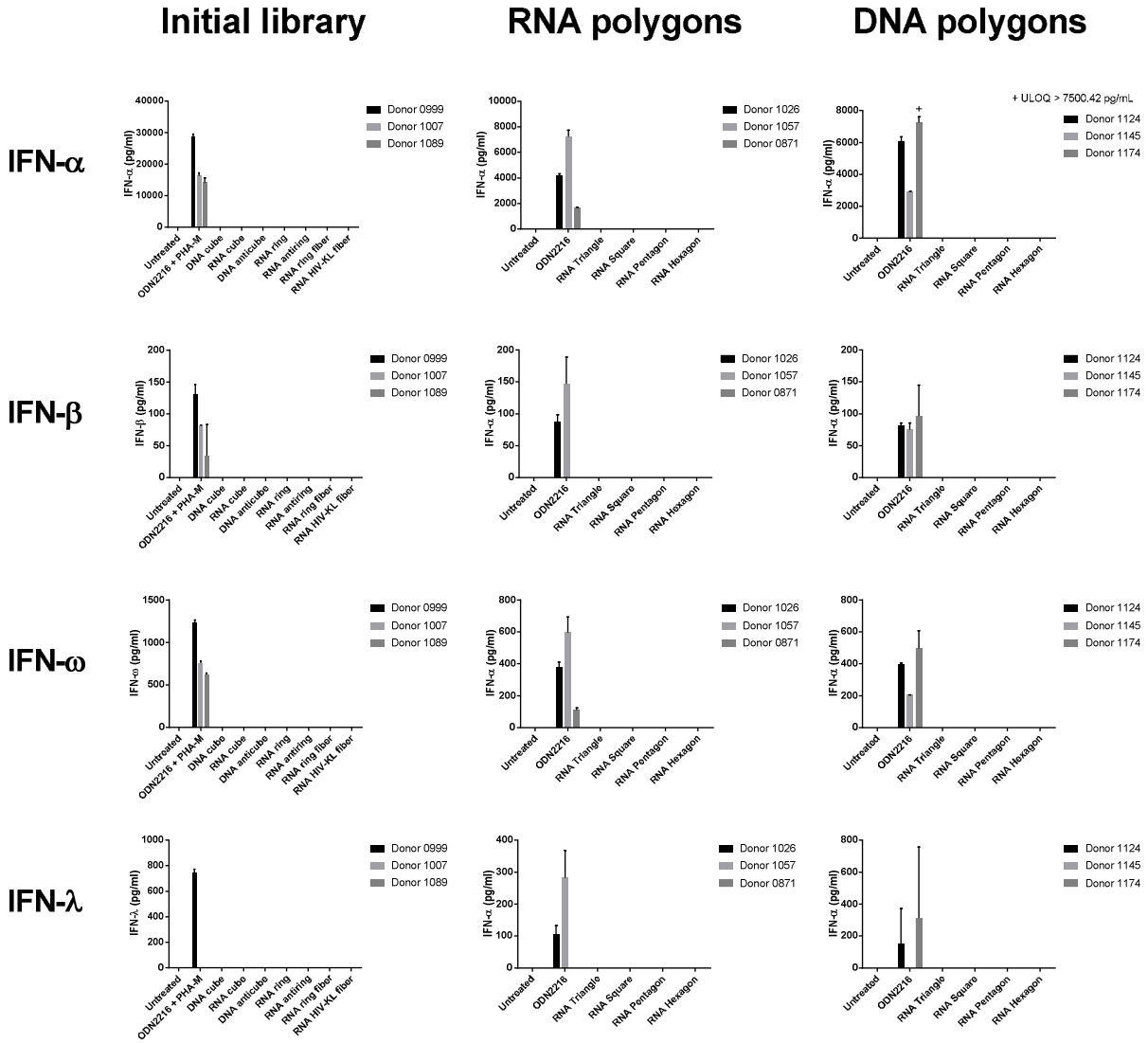


Figure S4. PBMCs treated with NANPs in the absence of L2K complexation. None of the NANPs induced any interferon (IFN) induction in the absence of L2K.

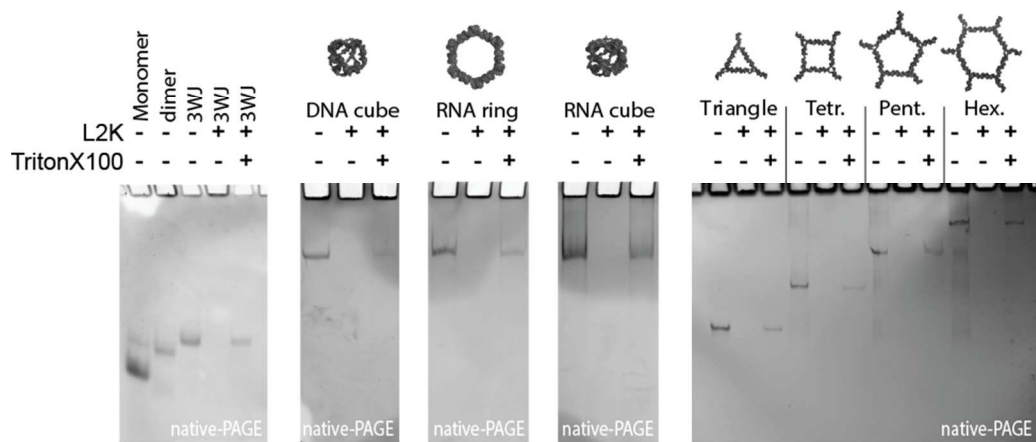


Figure S5. The structural integrity of NANPs is confirmed by Triton X-100-assisted release of NANPs from complexation with L2K. A stepwise assembly of the 3WJ domain from phi29 pRNA (denoted as “3WJ”) is also shown.

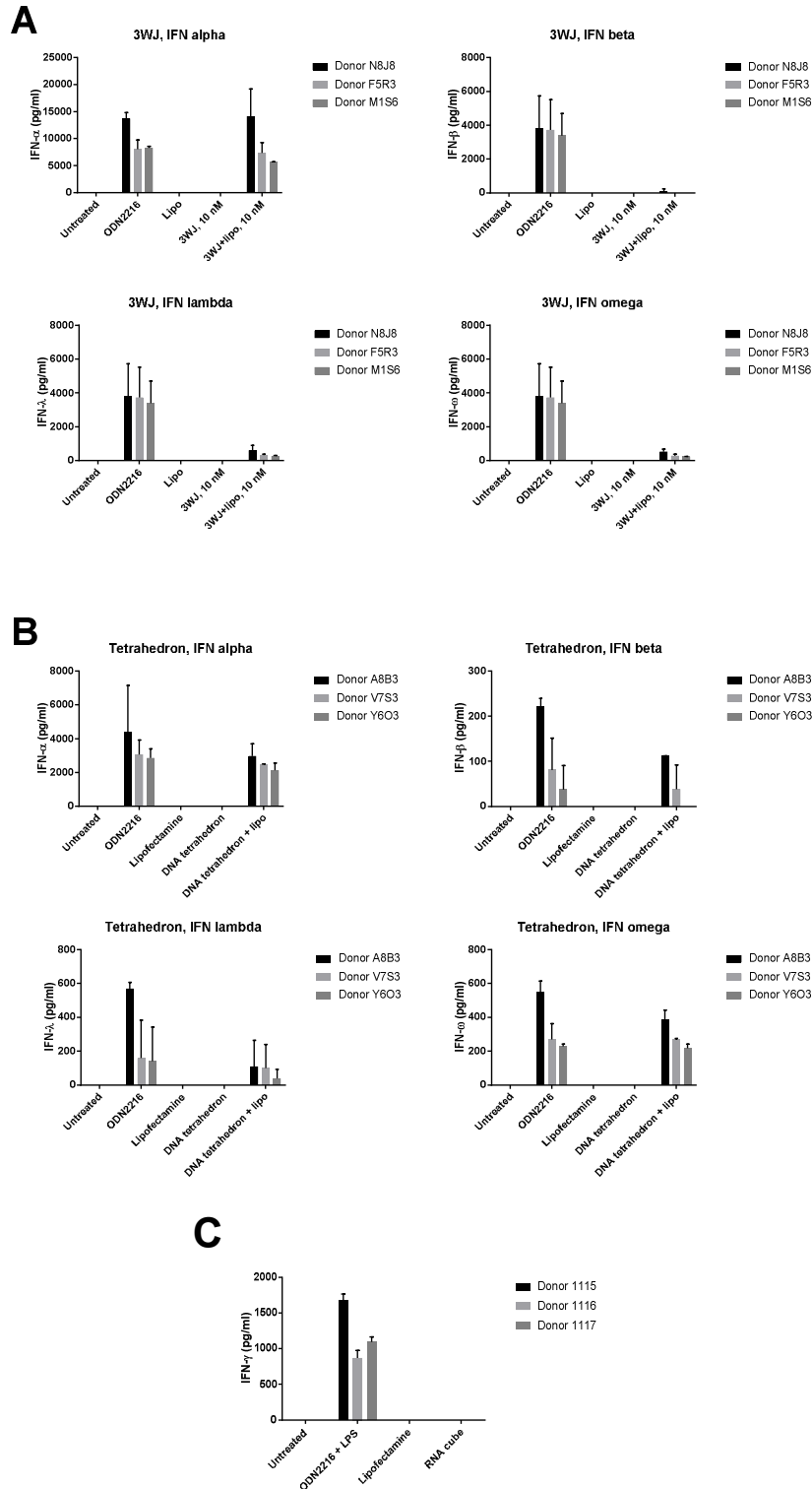


Figure S6. Interferon induction from PBMCs by RNA 3WJ and DNA tetrahedron NANPs designed by other groups. Previously published RNA three-way junction (3WJ) (A) and DNA tetrahedron (B) NANPs only induce type I and type III interferons in PBMCs upon L2K-mediated delivery. C: RNA cubes do not induce type II interferon (IFN- γ) production from whole blood.

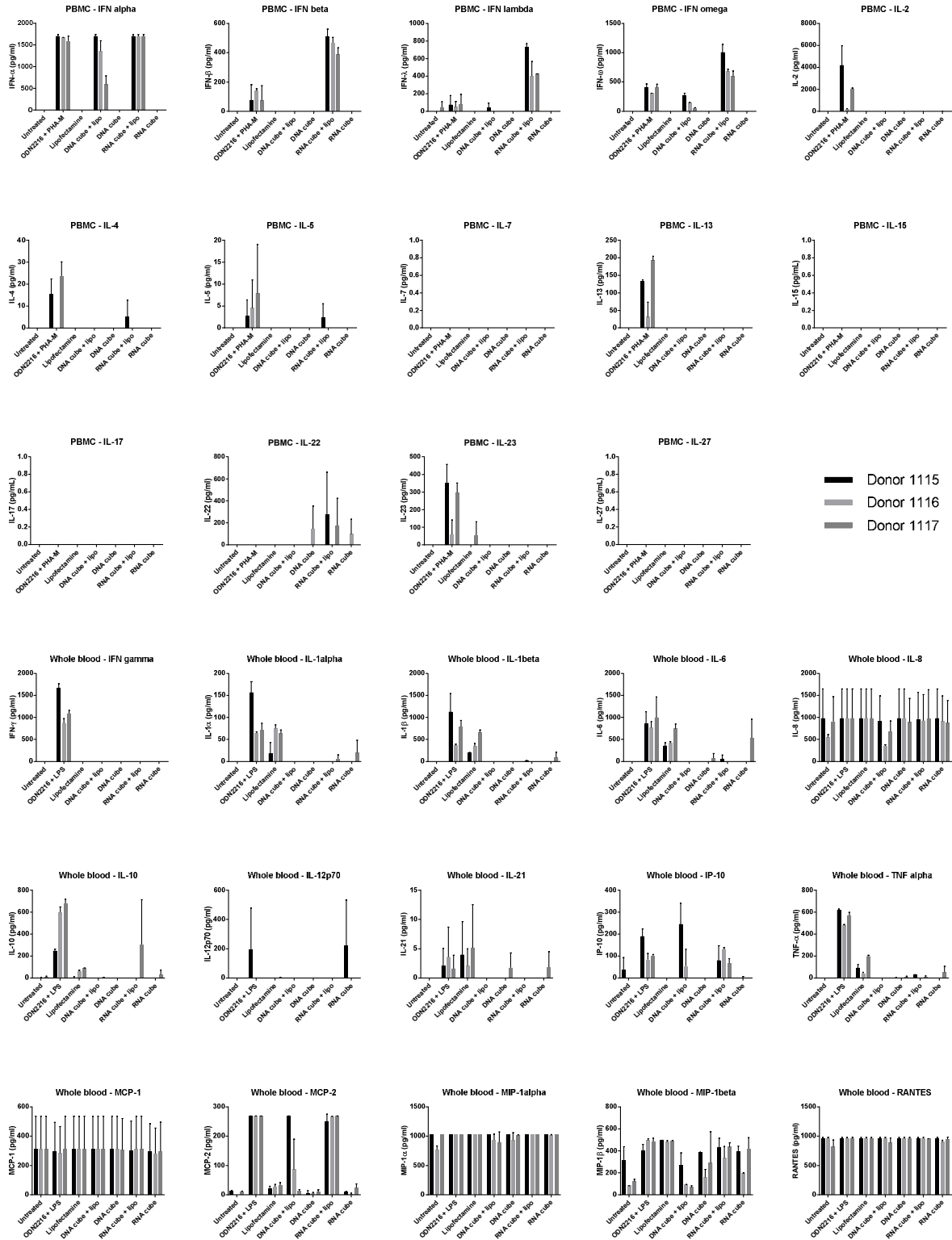


Figure S7. Multiplexed ELISA assaying for 29 different cytokines stimulated by DNA or RNA cubes, from PBMCs or whole blood.

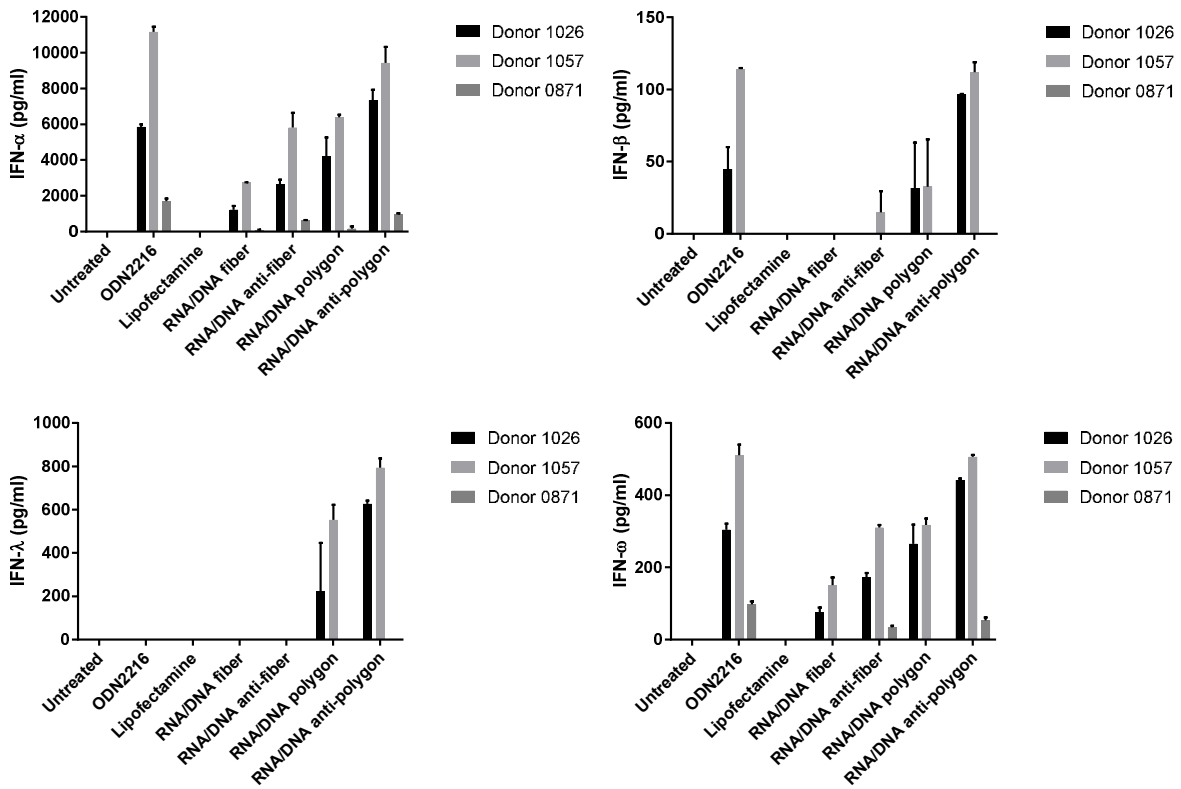


Figure S8. Interferon induction by PBMCs in response to fibers and polygons. NANPs at an equimolar concentration of 10 nM were delivered to PBMCs using Lipofectamine. IFN levels were measured in supernatants 24 hours after treatment.

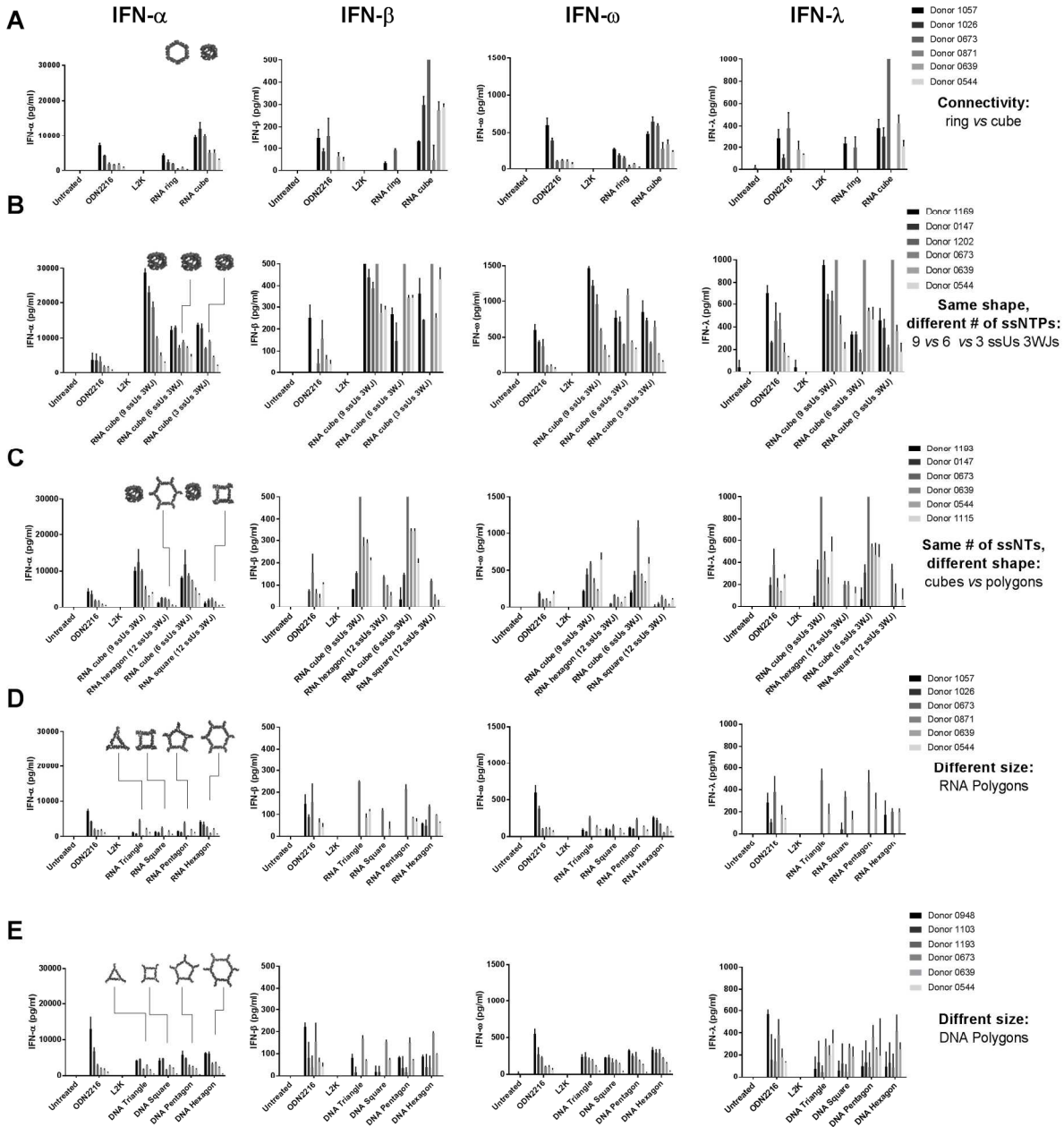


Figure S9. NANPs' connectivity and size contribute to interferon induction in PBMCs from 11 different donors. Bar graphs show the production of IFNs by PBMCs after delivery of NANPs with L2K to PBMCs. **A:** Comparison of NANPs with similar size but different connectivity. IFN stimulation by RNA cubes is stronger than that by RNA rings. **B:** Comparison of NANPs with similar shape but different ssNTs. RNA cubes with nine-ssU 3WJs are more immunostimulatory than cubes with fewer ssUs. **C:** Comparison of NANPs with the same number of ssNTs but different shape. When number of ssUs are kept constant, 3D globular RNA NANPs (cubes) are more immunostimulatory than planar NANPs (polygons). **D:** RNA hexagons stimulate the greatest amount of IFN compared to smaller RNA polygons with fewer 3WJs. **E:** DNA polygons show no relationship between size, number of 3WJs, and IFN induction. Each bar shows a mean response and standard deviation from experimental duplicates ($n = 3$ donors).

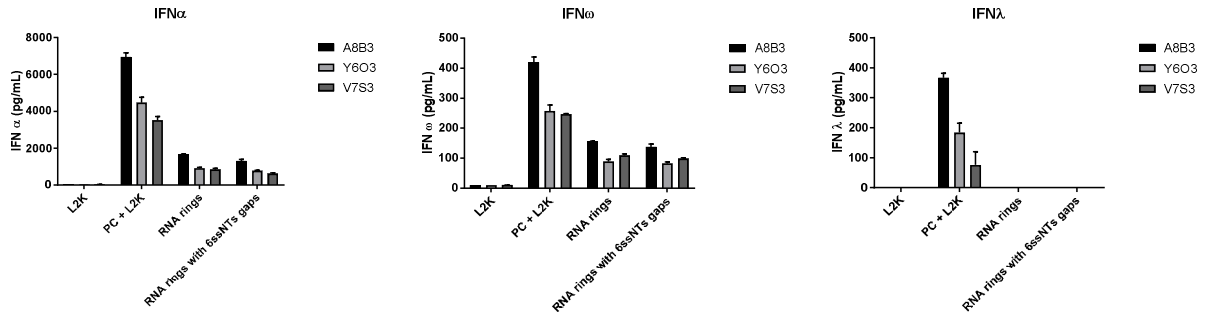


Figure S10. Interferon induction from PBMCs by RNA rings with a different number of ssNTs. All particles were tested at the equimolar concentration (10 nM) and delivered to PBMCs using Lipofectamine. Untreated cells and cells treated with ODN 2216 (PC) resulted in the same response as cells treated with vehicle only (L2K) and ODN 2216 in the presence of vehicle (PC+L2K). For simplicity, shown is baseline and PC data with L2K because this vehicle was also present in all nanoparticle-treated cells.

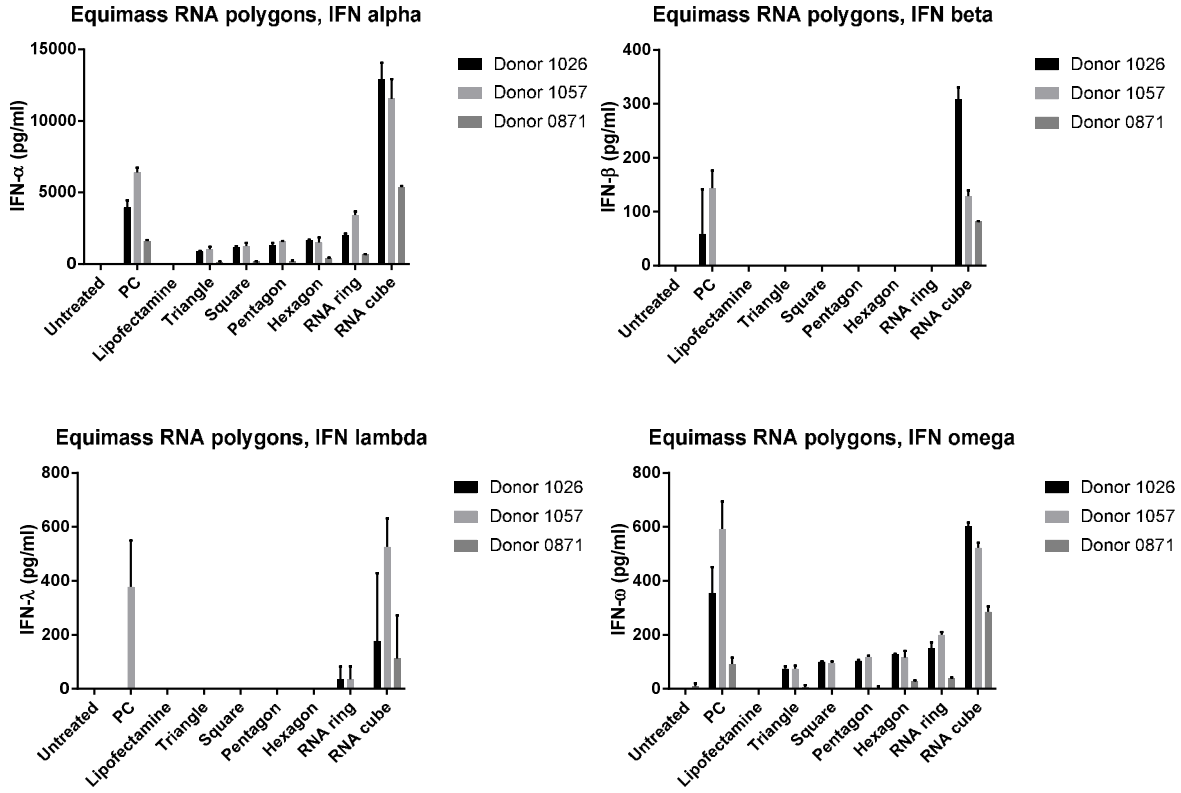


Figure S11. Interferon induction from PBMCs by RNA polygons at equal mass. RNA polygons were normalized to total nanoparticle mass at 10 nM of RNA squares (MW = 97 kDa), then delivered to PBMCs using Lipofectamine.

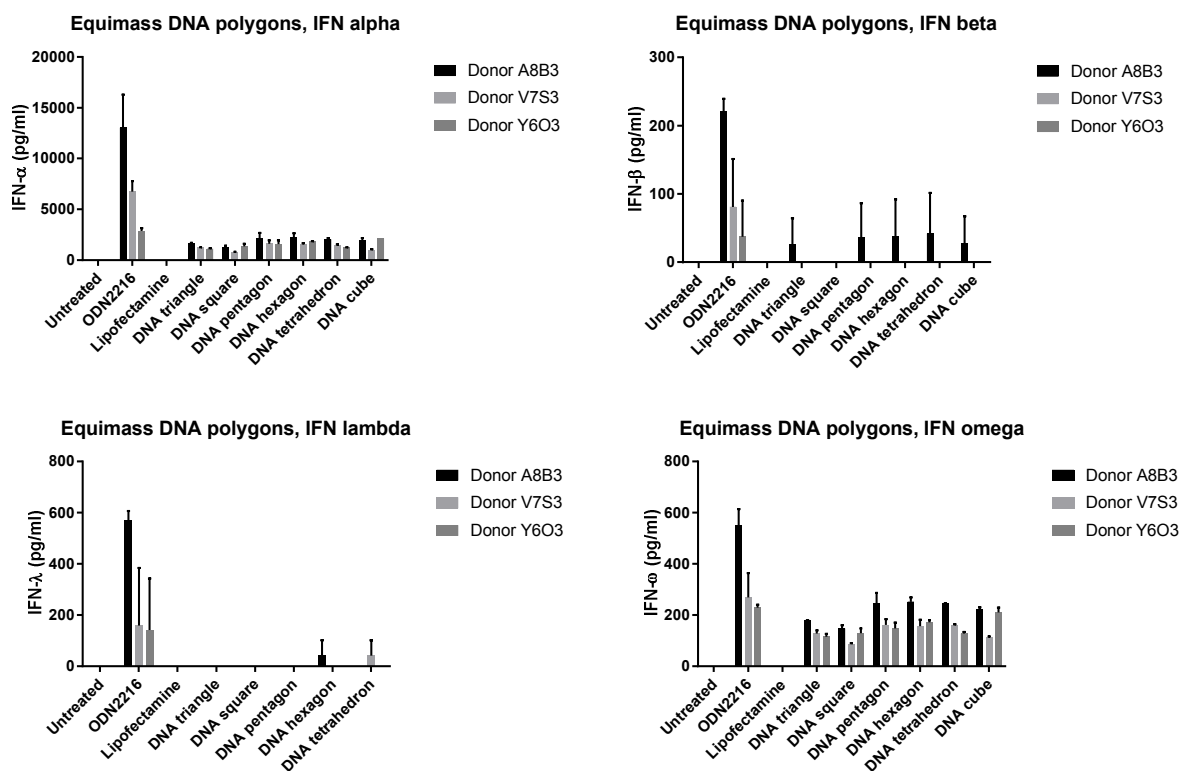


Figure S12. Interferon induction from PBMCs by DNA polygons at equal mass. DNA polygons were normalized to total nanoparticle mass at 10 nM of DNA squares (MW = 97 kDa), then delivered to PBMCs using Lipofectamine.

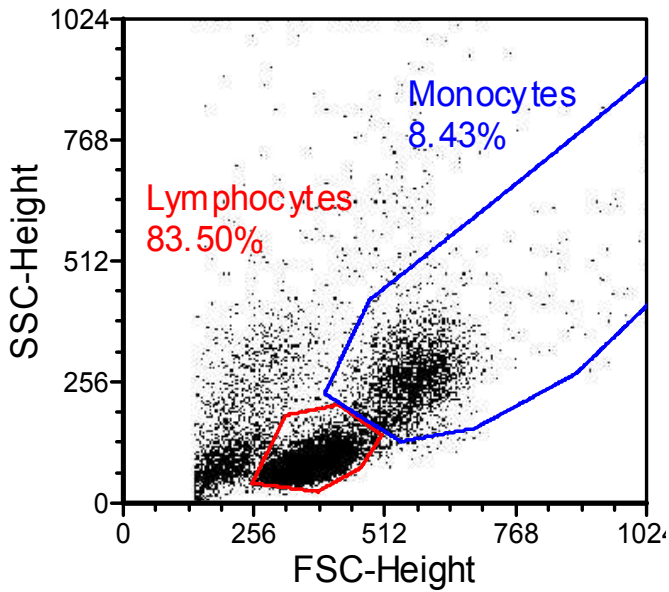


Figure S13. Distinguishing lymphocytes and monocytes by forward-scatter and side-scatter characteristics of PBMCs. Lymphocytes are identified by their low forward-scatter (size) and side-scatter (granularity) profiles, and they comprise the majority of PBMCs. Monocytes are identified by their higher forward- and side-scatter profiles. Cells gated in this manner are subsequently analyzed for nanoparticle association.

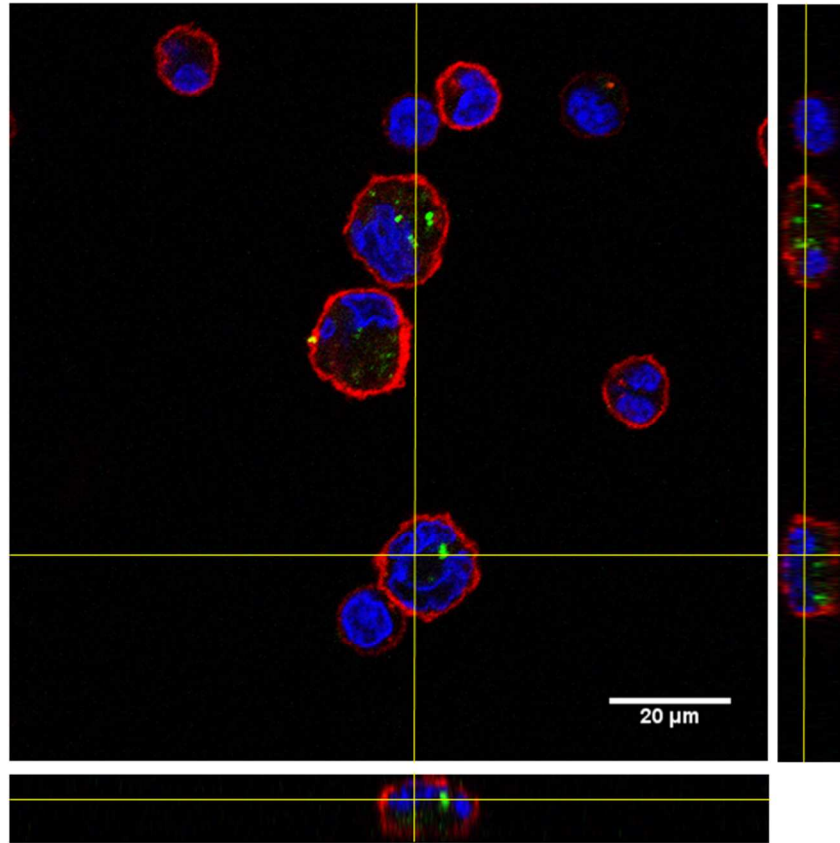


Figure S14. Orthogonal projection of z-stacked confocal image from PBMCs. PBMCs were treated with AF488-labeled RNA cubes, then stained with WGA 594 and imaged by confocal microscopy. Z-stacks were taken at 1 μm intervals. Yellow lines represent the projections across which the images are taken.

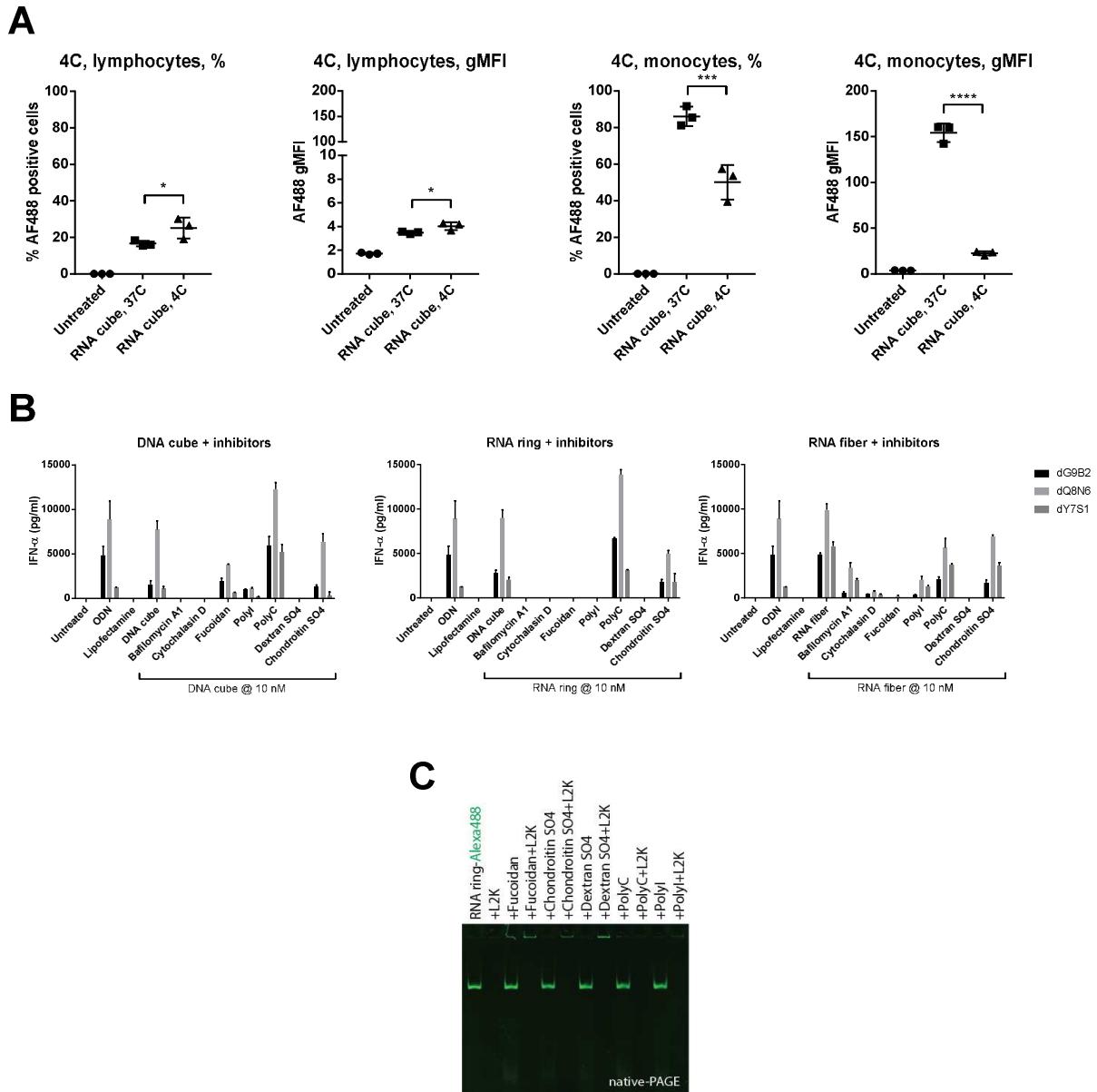


Figure S15. Effect of 4°C incubation on RNA cube internalization, as well as treatment with internalization and scavenger receptor inhibitors on different NANP types. **A:** PBMCs were treated with AF488-labeled RNA cubes overnight at either 37°C or 4°C, then assayed for NANP-associated fluorescence. Incubation at 4°C significantly reduced monocyte-associated fluorescence compared to 37°C treatment. Three donors were tested, with each dot representing data from an individual donor. Donor numbers = 1083, 1094, and 1150. **B:** PBMCs were treated with scavenger receptor inhibitors, then treated with DNA cubes (left panel), RNA rings (middle panel), or RNA fibers (right panel) and assayed for IFN- α production. **D:** The scavenger receptor inhibitors have no effect on naked NANPs, nor on the complexation of NANPs with L2K.

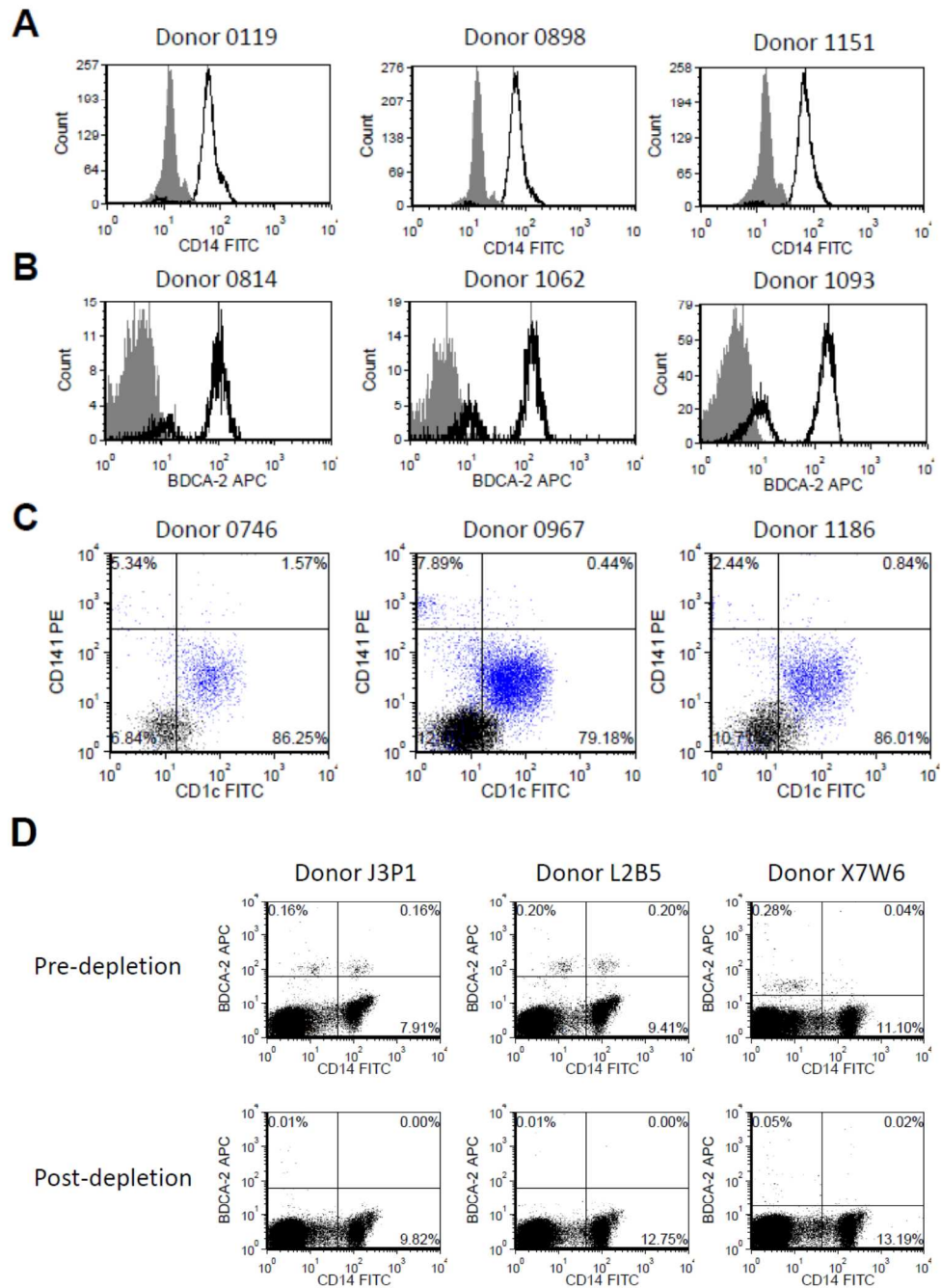


Figure S16. Phenotyping of purified DC subsets. Phenotyping of purified cells for each donor is shown in individual plots for the following DC subsets: **(A)** monocytes, **(B)** plasmacytoid dendritic cells (pDCs), and **(C)** myeloid dendritic cells. Monocytes are identified by staining with CD14 FITC, pDCs by BDCA-2 APC, and myeloid DCs by CD1c FITC and BDCA-3 PE. For **(A)** monocytes and **(B)** pDCs, black histograms represent purified cells stained with specific antibodies, while filled gray histograms represent purified cells stained with isotype control antibodies. For **(C)** myeloid DCs, blue dot plots represent purified cells stained with specific antibodies, while black dot plots represent purified cells stained with isotype control antibodies. **D:** Phenotyping of PBMCs before and after depletion of pDCs using CD304⁺ beads.

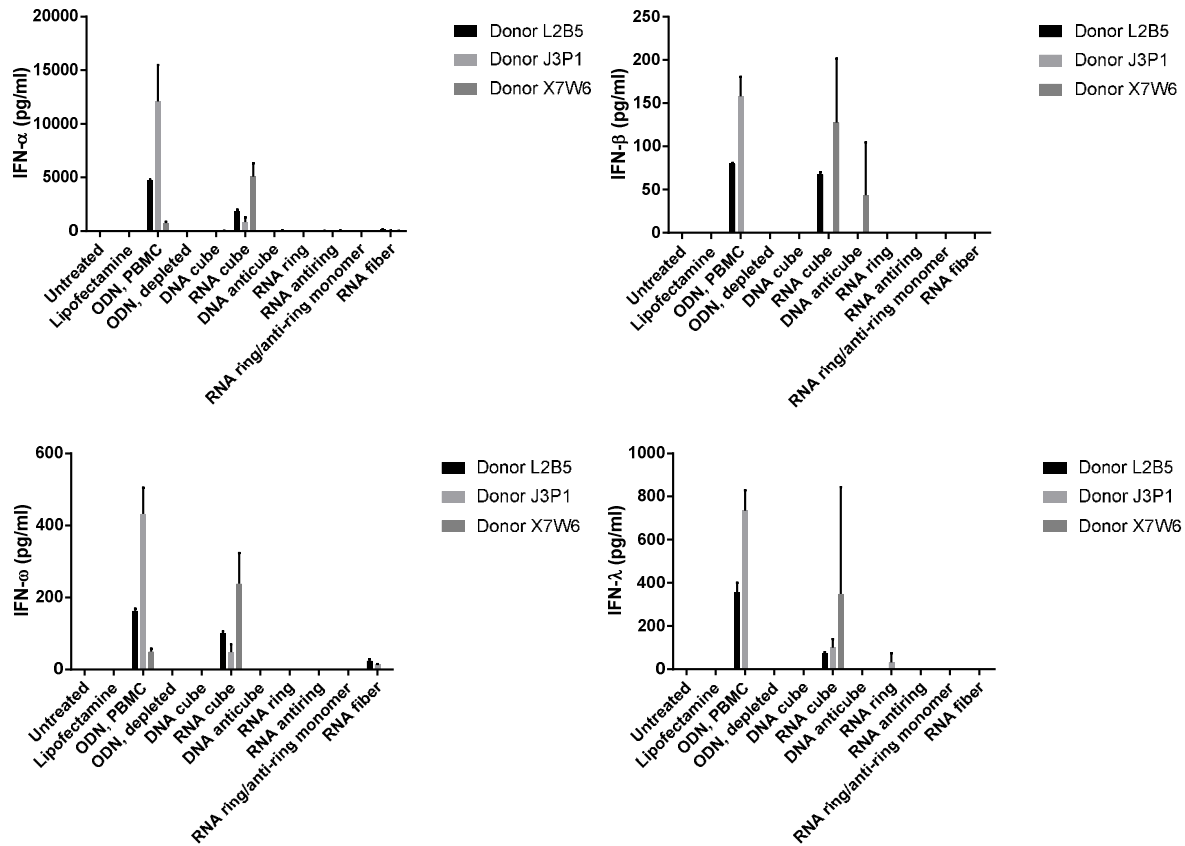


Figure S17. IFN response of PBMCs after pDC depletion. Plasmacytoid DCs were depleted using CD304⁺ beads. Then, the remaining cells were treated with NANPs and assayed for IFN induction by multiplexed ELISA.

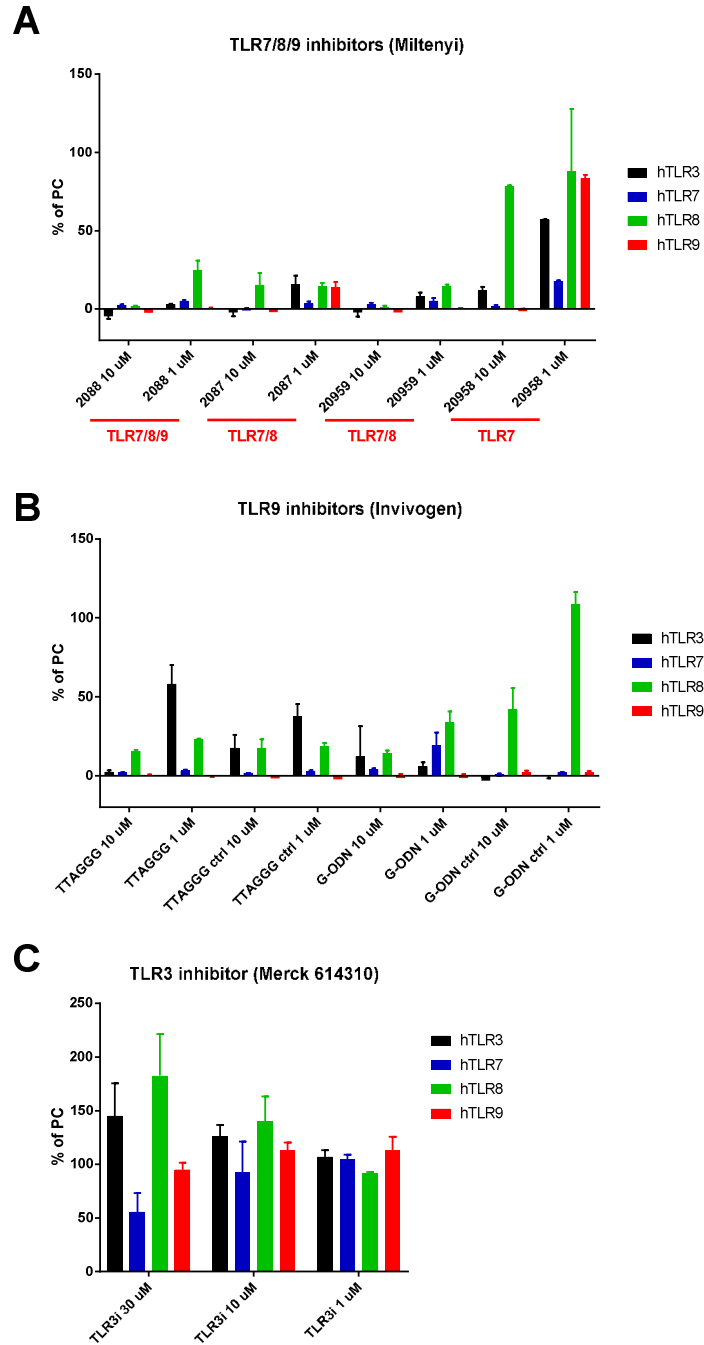


Figure S18. Validation of TLR inhibitors using a TLR reporter cell assay. A library of commercially available TLR inhibitors was validated for their specificity towards endosomal TLRs. Reporter cells overexpressing human TLR3, TLR7, TLR8, and TLR9 were treated with specific agonists (Poly(I:C), Imiquimod, ssRNA40/LyoVec, and ODN 2006, respectively) in the presence of TLR inhibitors for 24 hours. Resulting SEAP induction was normalized to SEAP induction for each individual cell line in the absence of inhibitor.

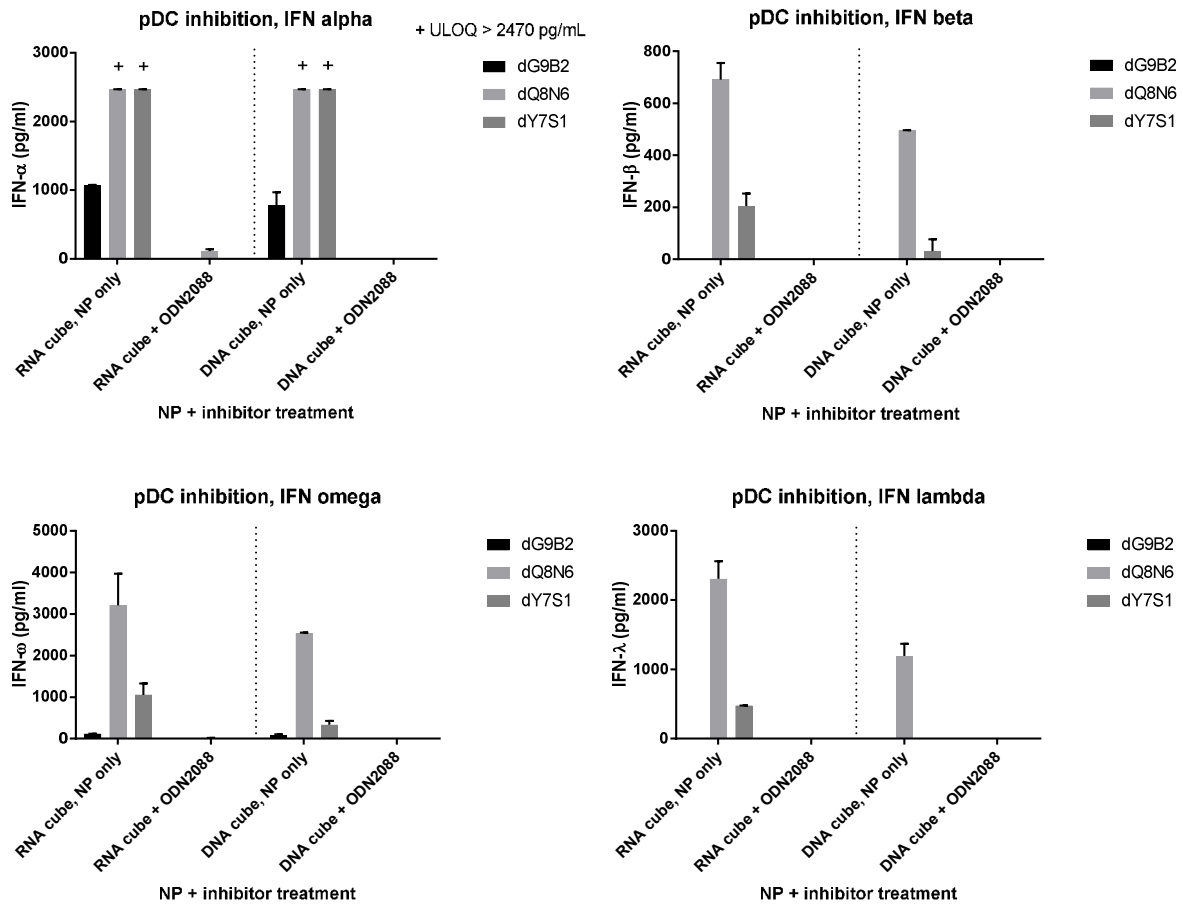


Figure S19. Inhibition of purified pDC IFN responses by ODN 2088. The addition of ODN 2088 abrogates the IFN response to DNA and RNA cubes in purified pDCs.

SUPPORTING TABLES

TABLE S1

NANPs	Size (d, nm)	±STDV	Tm (°C)	±STDV	Endotoxin (EU/ml)	Endotoxin Spike Recovery (%)
DNA triangles	17.1	2.3	65.6	0.6	<0.05	94
DNA squares	21.9	1.9	61.6	0.2	<0.05	118
DNA pentagons	23.8	3.3	56	0.3	<0.05	108
DNA hexagons	32.6	4.3	56.2	0.1	<0.05	127
DNA cubes (9Ts 3WJ)	10.1	2.3	36.6	0.3	<0.05	122
DNA anti-cubes (9As 3WJ)	11.8	0.8	35.3	0.3	<0.05	142
DNA polygons (RNAant)	18.8	2	44.8	1	<0.05	153
DNA Polygons (RNAsense)	21.2	2.5	47.6	1.1	<0.05	153
DNA fibers (RNAsense)	vary		51.9	0.5	<0.05	162
DNA fibers (RNAant)	vary		42.8	1.0	<0.05	149
DNA Tetrahedrons	9.5	0.9	61.4	1.0	<0.05	102
RNA triangles	14.3	0.9	74.9	1.1	<0.05	102
RNA squares	17.6	2.6	68.1	0.2	<0.05	99
RNA pentagons	19.8	0.6	65.6	0.5	<0.05	99
RNA hexagons	26.2	1.4	64	0.2	<0.05	97
RNA cubes (9Us 3WJ)	11.8	0.9	55.5	0.4	<0.05	97
RNA anti-cubes (9As 3WJ)	8.9	0.7	56.7	0.3	<0.05	102
RNA cubes (6Us 3WJ)	11.3	1.5	56.5	0.1	<0.05	112
RNA cubes (3Us 3WJ)	8.6	1.3	51.1	0.7	<0.05	138
RNA fibers	vary		59.5	0.1	<0.05	166
RNA rings	18.1	1.6	39	0.5	<0.05	113
RNA anti-rings	20.1	1.3	38.4	0.1	<0.05	107
RNA rings with six-ssNTs gaps	16.5	2.6	43.5	0.3	<0.05	121
R/AR monomers	18.8	1.6	45.2	1	<0.05	101
pRNA 3WJs	6.0	2.5	50.9	0.4	<0.05	99

Table S1: Physicochemical parameters measured for NANPs tested in this work. LAL data demonstrate that NANPs are endotoxin-free. According to the US Pharmacopeia standard (USP BET 85) the results of the LAL test are valid when spike recovery is between 50 and 200%.

TABLE S2

Plasmacytoid DCs	% BDCA2 ⁺ purified cells		
	Donor 0814	Donor 1062	Donor 1093
	85.43	82.27	83.39
Monocytes	% CD14 ⁺ purified cells		
	Donor 0119	Donor 0898	Donor 1151
	92.02	94.93	94.26
Myeloid DCs	% CD1c ⁺ CD141 ⁻ / CD1c ⁻ CD141 ⁺ purified myeloid DCs		
	Donor 0746	Donor 0967	Donor 1186
	91.59	87.07	88.45
Plasmacytoid DC depletion	% BDCA2 ⁺ depleted cells		
	Donor J3P1	Donor L2B5	Donor X7W6
	96.88	97.50	78.13

Table S2. Phenotyping results from purification and depletion of mononuclear phagocyte system immune cell subsets from human PBMCs.

TABLE S3

	DNA cube	RNA cube	DNA anti-cube	RNA ring	RNA anti-ring	RNA ring/anti-ring monomer	RNA fiber
ODN 2088	+++	+++	+++	+++	+++	+++	+++
ODN 2087	++	+++	+	+++	+++	+++	+++
ODN 20958	+++	-	++	+++	+++	+++	+++
ODN 20959	-	-	+	+++	+++	+++	+++
ODN TTAGGG	-	+++	-	+++	+++	+++	+++
ODN TTAGGG control	+	+++	-	+++	+++	+++	+++
G-ODN	+++	+++	+++	+++	+++	+++	+++
G-ODN control	+++	+++	+++	+++	+++	+++	+++
TLR3 inhibitor (Merck 614310)	-	-	-	-	-	-	-

Table S3. Effects of TLR inhibitors on IFN- α and IFN- ω responses in PBMCs. Legend: +++ = >90% inhibition, ++ = 50–90% inhibition, + = 25–50% inhibition, - = 0–25% inhibition.

REFERENCES:

1. Johnson, M.B., et al., *Programmable Nucleic Acid Based Polygons with Controlled Neuroimmunomodulatory Properties for Predictive QSAR Modeling*. Small, 2017.
2. Halman, J.R., et al., *Functionally-interdependent shape-switching nanoparticles with controllable properties*. Nucleic Acids Res, 2017.
3. Afonin, K.A., et al., *Computational and experimental characterization of RNA cubic nanoscaffolds*. Methods, 2014. **67**(2): p. 256-65.
4. Rose, S.D., et al., *Functional polarity is introduced by Dicer processing of short substrate RNAs*. Nucleic Acids Res, 2005. **33**(13): p. 4140-56.
5. Shu, D., et al., *Thermodynamically stable RNA three-way junction for constructing multifunctional nanoparticles for delivery of therapeutics*. Nat Nanotechnol, 2011. **6**(10): p. 658-67.
6. Goodman, R.P., R.M. Berry, and A.J. Turberfield, *The single-step synthesis of a DNA tetrahedron*. Chem Commun (Camb), 2004(12): p. 1372-3.